Table 1. Experimental (*28*) and theoretically estimated (Brownian dynamics) bimolecular rate constants k_2 (M^{-1} s^{-1}) for the cytochrome b_5 self-exchange ET as a function of ionic strength μ.

μ (M)	k_2 (M^{-1} s^{-1})	
	Experiment	Theory
0.1	2.6×10^3	1.0×10^3
0.3	4.6×10^3	2.4×10^4
0.6	1.6×10^4	7.6×10^4
1.0	2.8×10^4	1.1×10^5
1.5	4.5×10^4	1.7×10^5

extended-Hückel approach to electronic coupling calculation is certainly dependent on its parameterization.

The existence of multiple tunneling regimes also provides insight into several recent (and otherwise puzzling) experimental and theoretical observations in biological ET reaction kinetics. Winkler, Gray, and co-workers found that ET across protein-protein interfaces in protein crystals mediated by three water molecules is nearly as rapid as unimolecular ET is over the same distance (*7*). Canters and co-workers showed that water dimers between covalently cross-linked azurin complexes could substantially enhance the intermolecular ET kinetics (*15*). Similarly, Klinman and co-workers investigated the copper-to-copper ET over about 7 Å in the hydroxylating domain of peptidylglycine α-amidylating monooxygenase and found an unusually large electronic coupling mediated, apparently, by water rather than by the protein or substrate (*17*). Using Pathways-level analysis, Onuchic and co-workers found that water molecules mediate the dominant ET coupling routes between cytochrome c_2 and the photosynthetic reaction center (*18*). Cave and co-workers showed that water molecules between model D and A pairs substantially enhance intermolecular ET rates as well (*19*). All of these recent observations support our conclusion that a small number of structured water molecules interposed between the donor and the acceptor cofactors can substantially enhance ET rates.

The influence of aqueous tunneling pathways on interprotein ET kinetics has remained a key open issue in biological ET for some time. Single-exponential decay models fail to describe water-mediated ET reactions properly. The existence of multiple tunneling mediating regimes identified above is evinced by a body of recent experimental and theoretical observations. Most importantly, the structured water coupling regime may provide an important mechanism to facilitate ET reactions in the critical near-contact distance range relevant to biological ET kinetics. We hypothesize that water may be a particularly strong tunneling mediator when it occupies a sterically constrained space between redox cofactors with strong organizing forces that favor constructively interfering coupling pathways. It will be particularly interesting to use both theory and experiment to explore how the water-mediated coupling between proteins varies with protein-protein shape complementarity, surface charge and polarity, and dynamical fluctuations of the proteins and of the organized water at the interface.

References and Notes

1. J. M. Berg, L. Stryer, J. L. Tymoczko, *Biochemistry* (Freeman, New York, ed. 5, 2002).
2. H. B. Gray, J. R. Winkler, *Proc. Natl. Acad. Sci. U.S.A.* **102**, 3534 (2005).
3. Z. X. Liang *et al.*, *J. Am. Chem. Soc.* **126**, 2785 (2004).
4. A. Osyczka, C. C. Moser, F. Daldal, P. L. Dutton, *Nature* **427**, 607 (2004).
5. H. B. Gray, J. R. Winkler, *Q. Rev. Biophys.* **36**, 341 (2003).
6. R. E. Blankenship, *Nat. Struct. Biol.* **8**, 94 (2001).
7. F. A. Tezcan, B. R. Crane, J. R. Winkler, H. B. Gray, *Proc. Natl. Acad. Sci. U.S.A.* **98**, 5002 (2001).
8. G. McLendon, R. Hake, *Chem. Rev.* **92**, 481 (1992).
9. R. A. Marcus, N. Sutin, *Biochim. Biophys. Acta* **811**, 265 (1985).
10. S. S. Skourtis, I. A. Balabin, T. Kawatsu, D. N. Beratan, *Proc. Natl. Acad. Sci. U.S.A.* **102**, 3552 (2005).
11. I. A. Balabin, J. N. Onuchic, *Science* **290**, 114 (2000).
12. M. Jones, I. V. Kurnikov, D. N. Beratan, *J. Phys. Chem. A* **106**, 2002 (2002).
13. C. C. Page, C. C. Moser, X. X. Chen, P. L. Dutton, *Nature* **402**, 47 (1999).
14. M.-L. Tan, I. A. Balabin, J. N. Onuchic, *Biophys. J.* **86**, 1813 (2004).
15. I. M. C. van Amsterdam *et al.*, *Nat. Struct. Biol.* **9**, 48 (2002).
16. R. N. Barnett, C. L. Cleveland, U. Landman, G. B. Schuster, *Science* **294**, 567 (2001).
17. W. A. Francisco, G. Wille, A. J. Smith, D. J. Merkler, J. P. Klinman, *J. Am. Chem. Soc.* **126**, 13168 (2004).
18. O. Miyashita, M. Y. Okamura, J. N. Onuchic, *Proc. Natl. Acad. Sci. U.S.A.* **102**, 3558 (2005).
19. N. E. Miller, M. C. Wander, R. J. Cave, *J. Phys. Chem. A* **103**, 1084 (1999).
20. O. S. Wenger, B. S. Leigh, R. M. Villahermosa, H. B. Gray, J. R. Winkler, *Science* **307**, 99 (2005).
21. A. Ponce, H. B. Gray, J. R. Winkler, *J. Am. Chem. Soc.* **122**, 8187 (2000).
22. I. Benjamin, D. Evans, A. Nitzan, *J. Chem. Phys.* **106**, 6647 (1997).
23. M. D. Newton, *J. Electroanal. Chem.* **438**, 3 (1997).
24. S. Larsson, *J. Phys. Chem.* **88**, 1321 (1984).
25. J. R. R. Verlet, A. E. Bragg, A. Kammrath, O. Cheshnovsky, D. M. Neumark, *Science* **307**, 93 (2004).
26. K. Onda *et al.*, *Science* **308**, 1154 (2005).
27. R. C. E. Durley, F. S. Mathews, *Acta Crystallogr.* **D52**, 65 (1996).
28. S. M. Andrew, K. A. Thomasson, S. H. Northrup, *J. Am. Chem. Soc.* **115**, 5516 (1993).
29. S. H. Northrup, J. O. Boles, J. C. L. Reynolds, *Science* **241**, 67 (1988).
30. P. Strittmatter *et al.*, *Proc. Natl. Acad. Sci. U.S.A.* **71**, 4565 (1974).
31. E. Hegesh, J. Hegesh, A. N. Kaftory, *N. Engl. J. Med.* **314**, 757 (1986).
32. R. E. Utecht, D. M. Kurtz Jr., *Biochim. Biophys. Acta* **953**, 164 (1988).
33. D. W. Dixon, X. Hong, S. E. Woehler, A. G. Mauk, B. P. Sishta, *J. Am. Chem. Soc.* **112**, 1082 (1990).
34. W. L. Jorgensen, J. Chandrasekhar, J. D. Madura, R. W. Impey, M. L. Klein, *J. Chem. Phys.* **79**, 926 (1983).
35. Details of system setup, electronic structure, molecular dynamics, and Brownian dynamics simulations are available on *Science* Online.
36. T. Kawatsu, T. Kakitani, T. Yamato, *J. Phys. Chem. B* **106**, 5068 (2002).
37. P. Siddarth, R. A. Marcus, *J. Phys. Chem.* **97**, 1308 (1993).
38. D. N. Beratan, J. N. Betts, J. N. Onuchic, *Science* **252**, 1285 (1991).
39. H. Flyvbjerg, H. G. Petersen, *J. Chem. Phys.* **91**, 461 (1989).

40. This work was supported by the NIH (GM-048043). We are grateful to H. B. Gray and J. R. Winkler for stimulating discussions. We thank T. Kawatsu for providing code for the XH calculations, I. V. Kurnikov for providing code for the Pathways-based and atomic packing density-based calculations, and M. A. Pasquinelli for assistance with the Brownian dynamics calculations.

Supporting Online Material

www.sciencemag.org/cgi/content/full/310/5752/1311/DC1
SOM Text
Figs. S1 to S6
References

2 August 2005; accepted 20 October 2005
10.1126/science.1118316

Stable Carbon Cycle–Climate Relationship During the Late Pleistocene

Urs Siegenthaler,[1] Thomas F. Stocker,[1]* Eric Monnin,[1] Dieter Lüthi,[1] Jakob Schwander,[1] Bernhard Stauffer,[1] Dominique Raynaud,[2] Jean-Marc Barnola,[2] Hubertus Fischer,[3] Valérie Masson-Delmotte,[4] Jean Jouzel[4]

A record of atmospheric carbon dioxide (CO_2) concentrations measured on the EPICA (European Project for Ice Coring in Antarctica) Dome Concordia ice core extends the Vostok CO_2 record back to 650,000 years before the present (yr B.P.). Before 430,000 yr B.P., partial pressure of atmospheric CO_2 lies within the range of 260 and 180 parts per million by volume. This range is almost 30% smaller than that of the last four glacial cycles; however, the apparent sensitivity between deuterium and CO_2 remains stable throughout the six glacial cycles, suggesting that the relationship between CO_2 and Antarctic climate remained rather constant over this interval.

The European Project for Ice Coring in Antarctica (EPICA) recovered two deep ice cores from East Antarctica. One of the cores, located at Dome Concordia (Dome C) (75°06′S, 123°21′E, altitude of 3233 m above sea level, and mean annual accumulation rate of 25.0

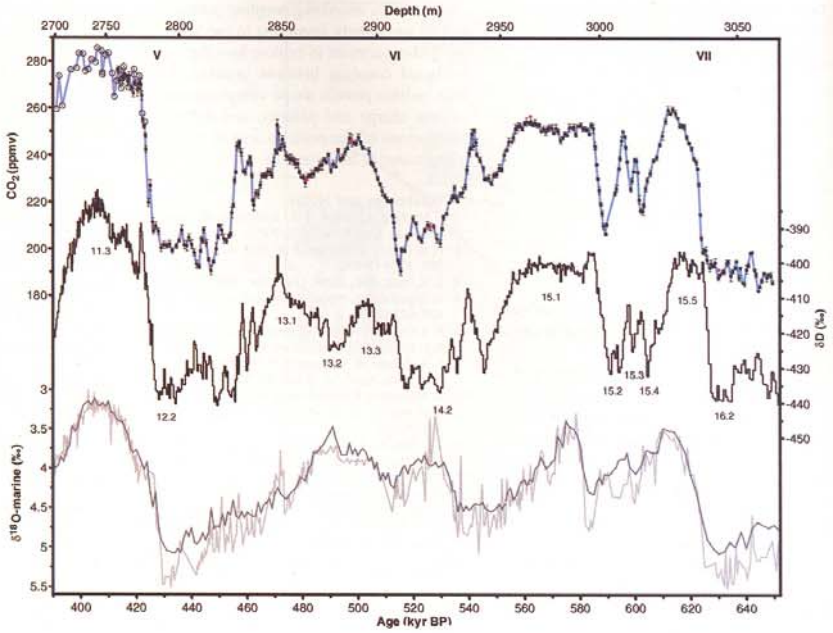

Fig. 1. Dome C CO_2 Bern data (black solid circles) are the mean of four to six samples, including the data from 31 depth intervals over termination V of (*1*); error bars denote 1σ of the mean. Red solid circles are test measurements with the use of the sublimation extraction technique. Dome C CO_2 Grenoble data are shown as black open circles. Dome C CO_2 measurements are connected with a blue line, and the high-resolution deuterium record is given as a black line (*18*). Benthic $\delta^{18}O$ stack and benthic $\delta^{18}O$ record from ODP site 980 are shown as a dark gray line (*19*) and a light gray line (*19–22*), respectively. The EDC2 time scale for Dome C is the same as in (*1*) (the depths at the top of the figure are only valid for the CO_2 record). Glacial terminations are given in roman numerals; marine isotope stages are given in arabic numerals according to (*17*).

kg m^{-2} $year^{-1}$), is the only ice core covering at least eight glacial cycles (*1*), four cycles longer than previously available from ice cores. This has allowed us to reconstruct the record of the concentration of atmospheric CO_2 much further back in time than was possible before. Here, we report results from the interval between 390 and 650 kyr B.P. (kyr B.P. is thousand years before the present, i.e., before A.D. 1950).

Analyzing the air extracted from ice cores is the only way to directly determine atmospheric greenhouse gas concentrations for times before routine atmospheric measurements were begun. Antarctic ice cores are very suitable for CO_2 measurements because of their low temperatures and low concentrations of impurities, which minimize the risk of artifacts. Data from different Antarctic ice cores (*2–13*) and drilled at sites with different temperatures, accumulation rates, and impurity concentrations [except cores with summer melting (*14*) and where elevated CO_2 values by up to 20 parts per million by volume (ppmv) are found] demonstrate that Antarctic ice cores are reliable recorders of atmospheric CO_2.

The concentrations of atmospheric CO_2 during the past four glacial cycles measured in the Vostok ice core vary between glacial and interglacial values of 180 ppmv and 280 to 300 ppmv, respectively (*7*). Including the data from Petit *et al.* (*7*), Fischer *et al.* (*5*) and Kawamura *et al.* (*10*), the lowest and highest values measured during a glacial cycle are on average 182 ± 4 ppmv (±1 standard deviation) and 296 ± 7 ppmv, respectively. This stable range of natural CO_2 variations on glacial-interglacial time scales led to the suggestion that feedbacks in the climate influence on the global carbon cycle maintain the rather narrow range observed (*15*).

The Dome C CO_2 record [mean sampling resolution of 731 years; details about the methods and the sampling are given in (*16*)] is plotted in Fig. 1, together with the δD record (Antarctic temperature proxy) of Dome C (*18*) [both records are shown on the EDC2 time scale (*1*)], a stack of benthic $\delta^{18}O$ records from globally distributed sites (*19*), and a high-resolution benthic $\delta^{18}O$ record from Ocean Drilling Project (ODP) site 980 (55°29′N, 14°42′W) (*19–22*). There is an excellent overall correlation between δD and benthic $\delta^{18}O$, a proxy of global ice volume (*19*).

First, we discuss the main features of the CO_2 record from Dome C from 650 to 390 kyr B.P. Our measurements begin at 650 kyr B.P., close to the lowest value for the entire record of 182 ppmv at 644 kyr B.P.. At marine isotope stage (MIS) 16, the CO_2 concentration is about 190 ppmv before the onset of termination VII. The entire transition between glacial and interglacial δD values occurred rapidly, within 3 kyear (ky) with the EDC2 dating. As expected from firnification processes, the corresponding CO_2 increase occurred deeper in the ice core, so there is no indication for an ice flow disturbance at this depth of about 3040 m, as has been observed at certain depths in the lowest 10% of some ice cores (*7*, *23*). After emerging slowly out of the baseline band, the CO_2 increase can be divided in two intervals. The first increase of 35 ppmv up to a CO_2 concentration of 235 ppmv takes less than 2 ky, whereas the second increase of another 20 ppmv takes about 5 ky. Although the CO_2 trend at the beginning of the interglacial MIS 15.5 does not show an early CO_2 peak as during the past four interglacials, this second CO_2 increase is very similar in magnitude (20 ppmv) and duration (5 ky) to the Holocene one, although evolving with generally lower CO_2 values by about 25 ppmv. Therefore, the Holocene increase during the last 8 kyear is not an anomalous trend in comparison to other interglacials as postulated recently (*24*); instead it is a likely response of the carbon cycle

[1]Climate and Environmental Physics, Physics Institute, University of Bern, Sidlerstrasse 5, CH-3012 Bern, Switzerland. [2]Laboratoire de Glaciologie et de Géophysique de l'Environnement (CNRS), 54 Rue Molières, 38402 St. Martin d'Hères Cedex, France. [3]Alfred Wegener Institute for Polar and Marine Research (AWI), Columbusstrasse, D-27568 Bremerhaven, Germany. [4]Institut Pierre Simon Laplace/Laboratoire des Sciences du Climat et de l'Environnement, CEA-CNRS 1572, CE Saclay, Orme des Merisiers, 91191 Gif-sur-Yvette, France.

*To whom correspondence should be addressed. E-mail: stocker@climate.unibe.ch

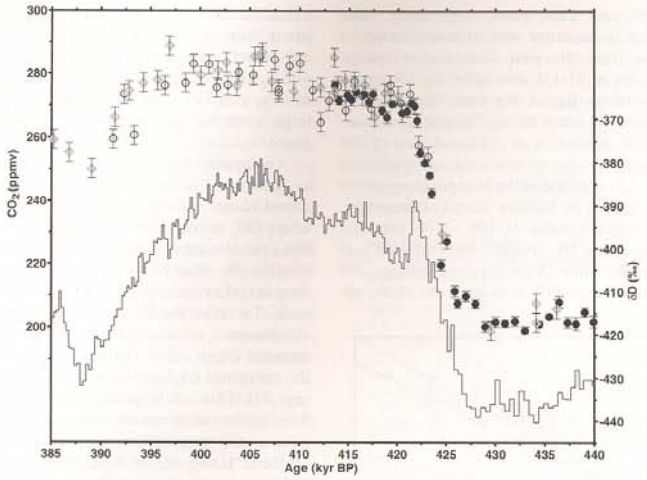

Fig. 2. CO_2 results of entire MIS 11, including end of MIS 12. Dome C CO_2 Bern data (solid circles) from EPICA community members (*7*) and this work; error bars, 1σ of the mean. Dome C CO_2 Grenoble data are indicated by open circles; error bars, accuracy of $2\sigma = 3$ ppmv. High-resolution deuterium record is shown as a black line (*18*). Vostok CO_2 Grenoble data are indicated by gray open diamonds; error bars, accuracy of $2\sigma = 3$ ppmv on the corrected time scale (*28*).

to large changes in biomass (*25*). At the end of MIS 15.5, CO_2 attains its local maximum of about 260 ppmv, which is the highest concentration in the record before MIS 11 but substantially lower than the interglacial concentrations measured during the last four glacial cycles. At MIS 15.4 and MIS 15.2, the deuterium record indicates near-glacial conditions, only interrupted by two peaks at MIS 15.3. During the time interval of MIS 15.4 to 15.2, CO_2 shows rather large variations, with values between 207 ppmv and 250 ppmv and with two peaks during MIS 15.3 that are very similar to the deuterium peaks. The lowest values are close to glacial CO_2 concentrations, which raise the question of whether MIS 15 was a single continuous interglacial or multiple ones.

The increases of CO_2 and δD into MIS 15.1 are very uniform and take 4 to 5 ky for each component. An unexpected feature is the very stable and long-lasting MIS 15.1. In contrast to the increasing global ice volume suggested by the benthic records of marine sediments (Fig. 1) (*19*), all indicators from Dome C exhibit almost constant values during MIS 15.1. This is observed in the records of deuterium (*1*), of CH_4 (*26*), and of aerosols (*27*) of the Dome C ice core but is most pronounced in our CO_2 results. We find a stable 251.5 ± 1.9 ppmv (±1 standard deviation) CO_2 concentration from 585 kyr B.P. to 557 kyr B.P. on the EDC2 time scale, which is unprecedented in any other time interval covered by previous CO_2 measurements on ice cores. This result suggests that the global carbon cycle operated in an exceptionally stable mode for many millennia. The current estimate for the duration of MIS 15.1, on the basis of the EDC2 time scale, is 28,000 years. Accordingly, this interval is a prime target for developing a better understanding of the influence of orbital geometry on climate and the global carbon cycle. However, we cannot, at this stage, exclude the possibility that at least part of the exceptionally long duration of stable conditions could be due to an exceptionally low thinning rate of the corresponding ice layer.

The decrease in δD from the end of MIS 15.1 to the start of MIS 14.2 is interrupted by a double peak, the older of which is most pronounced with a corresponding peak in the CO_2 record and with elevated values by more than 20 ppmv. The phase relationship between CO_2 and deuterium for this event is dicussed later in the text. The deuterium increase to the maximum value of MIS 13.3 ("termination" VI) evolves in two steps, with a rather stable concentration in between and a difference between glacial and interglacial values that is smaller in comparison to any other termination during the past 650 ky. The CO_2 increase can be divided again into two intervals, as for termination VII. The first increase of 30 ppmv takes 3 ky, whereas the duration for the second increase of 20 ppmv is more than 8 ky. During MIS 13, CO_2 values are in the range of about 230 to 250 ppmv, with a minimum at 481 kyr B.P. This minimum lags the deuterium minimum by about 10 ky. The decrease to MIS 12.2 is interrupted by another prominent set of deuterium and CO_2 double peaks. During MIS 12.2 (and also MIS 16.2) we find pronounced millennial CO_2 fluctuations of 10 to 20 ppmv. They are comparable in duration and amplitude to the distinct CO_2 peaks observed during the past four Antarctic warm events (A1 to A4) during the last glacial (*4*, *8*).

A detailed comparison with Vostok data (*28*) during MIS 11, an interglacial period that occurred some 400,000 years ago and lasted for about 30,000 years, is shown in Fig. 2 in order to examine the consistency of CO_2 values measured in this deep ice. Both records agree within the error limits and show interglacial CO_2 concentrations in MIS 11 similar to those found in the Holocene. Accordingly, we are confident that the Dome C data in the pre-Vostok era reflect true atmospheric CO_2 concentrations.

The coupling of CO_2 and δD is strong. The overall correlation between CO_2 data and Antarctic temperature during the time period of 390 to 650 kyr B.P. is $r^2 = 0.71$. Taking into account only the period 430 to 650 kyr B.P., where amplitudes of deuterium and CO_2 are smaller, the correlation is $r^2 = 0.57$. Corrections for changes in the temperature and δD of the water vapor source, which also affect δD of the ice, have not been made yet. The strong coupling of CO_2 to Antarctic temperature confirms earlier observations for the last glacial termination (*9*) and the past four glacial cycles (*7*) and supports the hypothesis that the Southern Ocean played an important role in causing CO_2 variations.

δD as a function of CO_2 from the Vostok (MIS 1 to MIS 11) and Dome C ice cores [MIS 12 to 16, Holocene (*11*), and termination I (*9*)] is shown in Fig. 3. The offset in the deuterium values of Dome C and Vostok is due to the different distances to the open ocean, elevations, and surface temperatures of the two sites (*29*). It is remarkable that the slope of the three records is essentially the same. This suggests that the coupling of Antarctic temperature and CO_2 did not change substantially during the last 650 ky.

Another important parameter elucidating the coupling of atmospheric CO_2 and Antarctic temperature is their relative phasing. Because of the enclosure process of air in ice, the phase relationship of CO_2 and δD is associated with uncertainties. Because the enclosed air is younger than the surrounding ice (*30*), CO_2 is plotted on a gas age chronology, whereas deuterium is plotted on an ice age chronology. For Dome C and the period under investigation, the gas age/ice age difference (Δ age) is in the range of 1.9 to 5.5 ky (fig. S1). The estimated uncertainty of Δ age in the upper 800 m of

the Dome C ice core is about 10% (*31*), neglecting uncertainties in the thinning rate. Deviations from the modeled thinning would introduce systematic errors in Δ age.

By shifting the time scales of the entire CO_2 and deuterium records between 390 and 650 kyr B.P. relative to each other, we obtained the best correlation for a lag of CO_2 of 1900 years. This lag is significant considering the uncertainties of Δ age. Over the glacial terminations V to VII, the highest correlation of CO_2 and deuterium, with use of a 20-ky window for each termination, yields a lag of CO_2 to deuterium of 800, 1600, and 2800 years, respectively. This value is consistent with estimates based on data from the past four glacial cycles. Fischer *et al.* (*5*) concluded that CO_2 concentrations lagged Antarctic warmings by 600 ± 400 years during the past three transitions. Monnin *et al.* (*9*) found a lag of 800 ± 600 years for termination I, and Caillon *et al.* (*32*), with use of the isotopic composition of argon in air bubbles instead of deuterium, calculated a value of 800 ± 200 years for termination III. Overall, the estimated lags over the entire Dome C record between 390 and 650 kyr B.P. and over the three terminations in this time period are small compared with glacial-interglacial time scales and do not cast doubt on the strong coupling of CO_2 and temperature or on the importance of CO_2 as a key amplification factor of the large observed temperature variations of glacial cycles.

An apparent exception of the lag of CO_2 to deuterium observed over most of the record occurs around 534 to 548 kyr B.P., where CO_2 seems to lead δD by about 2000 ± 500 year. We cannot conclude with certainty whether the observed lead of CO_2 at this time is real or an artefact in the EDC2 time scale. To make the CO_2 and the δD peaks simultaneous, we would need to increase the modeled depth offset of the gas record and the ice record (Δ depth) from 4.3 m to 7 m (fig. S2). This can be achieved by a reduced thinning rate, an increased accumulation rate, a decreased temperature, or a combination of them. However, because accumulation and temperature are strongly positively correlated at present (*33*), the required change in accumulation or temperature, or a change of both, is rather unlikely. An anomalously low thinning rate is therefore the more likely way to produce such an artefact in the EDC2 time scale.

A composite CO_2 record over six and a half ice age cycles back to 650,000 yr B.P. is shown in Fig. 4, created from a combination of records from the Dome C, Taylor Dome, and Vostok ice cores. This record shows the differences in amplitudes of CO_2 and deuterium before and after 430 kyr B.P. and demonstrates, within the resolution of our measurements, that the atmospheric concentration of CO_2 did not exceed 300 ppmv for the last 650,000 years before the preindustrial era.

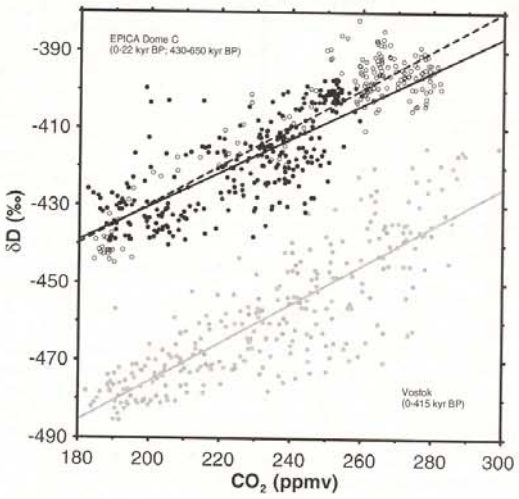

Fig. 3. Correlation between δD, a proxy for Antarctic temperature, and CO_2 for three data sets. The new data from Dome C cover the beginning of MIS 12 to MIS 16 (black solid circles; black line is the linear fit δD = 0.44‰ ppmv^{-1} × CO_2 − 517.75‰, r^2 = 0.57), and the period from MIS 1 to MIS 11 is covered by data from the Vostok ice core [gray solid circles (*7*); gray line is linear fit, δD = 0.50‰ ppmv^{-1} × CO_2 − 575.86‰, r^2 = 0.70] and Dome C Holocene and termination I [black open circles (*9*, *11*); black dashed line is the linear fit, δD = 0.50‰ ppmv^{-1} × CO_2 − 529.87‰, r^2 = 0.84]. The offset in the δD values from these two cores is due to the different distances to the open ocean, elevations, and surface temperatures of the two sites (*29*).

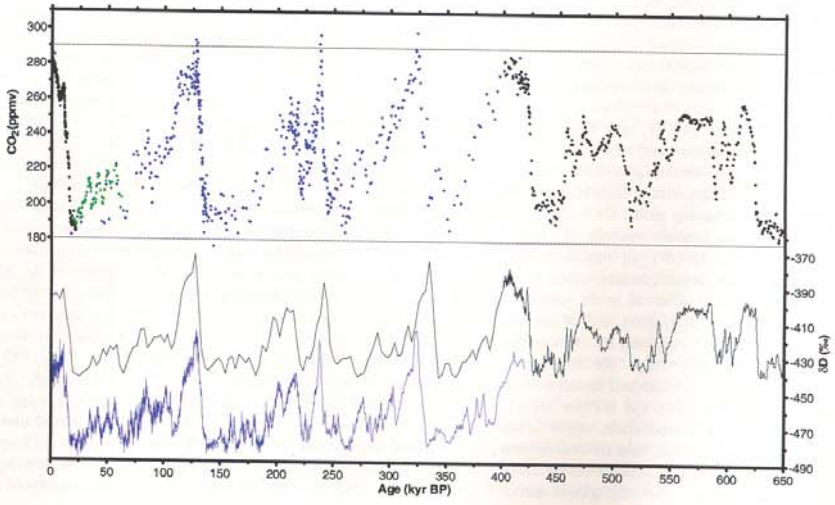

Fig. 4. A composite CO_2 record over six and a half ice age cycles, back to 650,000 years B.P. The record results from the combination of CO_2 data from three Antarctic ice cores: Dome C (black), 0 to 22 kyr B.P. (*9*, *11*) and 390 to 650 kyr B.P. [this work including data from 31 depth intervals over termination V of (*1*)]; Vostok (blue), 0 to 420 kyr B.P. (*5*, *7*), and Taylor Dome (light green), 20 to 62 yr B.P. (*8*). Black line indicates δD from Dome C, 0 to 400 kyr B.P. (*1*) and 400 to 650 kyr B.P. (*18*). Blue line indicates δD from Vostok, 0 to 420 kyr B.P. (*7*).

The CO_2 record from the EPICA Dome C ice core reveals that atmospheric CO_2 variations during glacial-interglacial cycles had a notably different character before and after 430 kyr B.P. Before MIS 11, the amplitude of temperature was lower, and the duration of the warm phases has been much longer since then. In spite of these differences, the significant covariation of δD and CO_2 is valid in both periods. Before MIS 11, CO_2 concentrations did not exceed 260 ppmv. This is substantially lower than the maxima of the last four glacial cycles. The lags of CO_2 with respect to the Antarctic temperature over glacial terminations V to VII are 800, 1600, and 2800 years, respectively, which are consistent with earlier observations during the last four glacial cycles.

Our measurements have revealed an unexpected stable climate phase (MIS 15.1) during which the atmospheric CO_2 concentration was 251.5 ± 1.9 ppmv for many millennia (28,000 years, based on the EDC2 time scale), although the duration of MIS 15.1 is uncertain because of possible inaccuracies in the Dome C EDC2 time scale between MIS 12 and 15. However, the roughly 30,000-year duration of MIS 11 (and possibly MIS 15.1) demonstrates that long interglacials with stable conditions are not exceptional. Short interglacials such as the past three therefore are not the rule and hence cannot serve as analogs of the Holocene, as postulated recently (*24*). Examining δD as a function of CO_2, we observe that the slope during the two new glacial cycles compared to the last four cycles is essentially the same. Therefore, the coupling of Antarctic temperature and CO_2 did not change significantly during the last 650 kyear, indicating rather stable coupling between climate and the carbon cycle during the late Pleistocene.

References and Notes

1. L. Augustin *et al.*, (EPICA community members), *Nature* **429**, 623 (2004).
2. J.-M. Barnola, D. Raynaud, Y. S. Korotkevich, C. Lorius, *Nature* **329**, 408 (1987).
3. D. M. Etheridge *et al.*, *J. Geophys. Res.* **101**, 4115 (1996).
4. B. Stauffer *et al.*, *Nature* **392**, 59 (1998).
5. H. Fischer, M. Wahlen, J. Smith, D. Mastroianni, B. Deck, *Science* **283**, 1712 (1999).
6. A. Indermühle *et al.*, *Nature* **398**, 121 (1999).
7. J. R. Petit *et al.*, *Nature* **399**, 429 (1999).
8. A. Indermühle, E. Monnin, B. Stauffer, T. F. Stocker, M. Wahlen, *Geophys. Res. Lett.* **27**, 735 (2000).
9. E. Monnin *et al.*, *Science* **291**, 112 (2001).
10. K. Kawamura *et al.*, *Tellus* **55B**, 126 (2003).
11. E. Monnin *et al.*, *Earth Planet. Sci. Lett.* **224**, 45 (2004).
12. U. Siegenthaler *et al.*, *Tellus* **57B**, 51 (2005).
13. J. Flückiger *et al.*, *Global Biogeochem. Cycles* **16**, 1010 (2002).
14. J. Ahn *et al.*, *J. Geophys. Res.* **109**, 10.1029/2003JD004415 (2004).
15. P. Falkowski *et al.*, *Science* **290**, 291 (2000).
16. Supplementary information concerning methods or assumptions is available on *Science* Online.
17. F. C. Bassinot *et al.*, *Earth Planet. Sci. Lett.* **126**, 91 (1994).
18. J. Jouzel *et al.*, in preparation.
19. L. E. Lisiecki, M. E. Raymo, *Paleoceanography* **20**, 10.1029/2004PA001071 (2005).
20. D. W. Oppo, J. F. McManus, J. L. Cullen, *Science* **279**, 1335 (1998).
21. J. F. McManus, D. W. Oppo, J. L. Cullen, *Science* **283**, 971 (1999).
22. B. P. Flower *et al.*, *Paleoceanography* **15**, 388 (2000).
23. A. Landais *et al.*, *J. Geophys. Res.* **109**, 10.1029/2003JD004193 (2004).
24. W. F. Ruddiman, *Clim. Change* **61**, 261 (2003).
25. F. Joos, S. Gerber, I. C. Prentice, B. L. Otto-Bliesner, P. J. Valdes, *Global Biogeochem. Cycles* **18**, 10.1029/2003GB002156 (2004).
26. R. Spahni *et al.*, *Science* **310**, 1317 (2005).
27. E. W. Wolff *et al.*, in preparation.
28. D. Raynaud *et al.*, *Nature* **436**, 39 (2005).
29. V. Masson *et al.*, *Quaternary Res.* **54**, 348 (2000).
30. J. Schwander, B. Stauffer, *Nature* **311**, 45 (1984).
31. J. Schwander *et al.*, *Geophys. Res. Lett.* **28**, 4243 (2001).
32. N. Caillon *et al.*, *Science* **299**, 1728 (2003).
33. J. Jouzel *et al.*, *Nature* **329**, 403 (1987).

34. We thank K. Kawamura and G. Teste for assisting with the CO_2 measurements, L. Lisiecki and M. Raymo for access to the data of (*19*), and R. Spahni and F. Parrenin for fruitful discussions. This work is a contribution to the EPICA, a joint European Science Foundation/European Commission (EC) scientific program funded by the EC and by national contributions from Belgium, Denmark, France, Germany, Italy, Netherlands, Norway, Sweden, Switzerland, and United Kingdom. We acknowledge long-term financial support by the Swiss National Science Foundation, the University of Bern, the Swiss Federal Office of Energy, and EC Project EPICA-MIS. This is EPICA publication no. 133.

Supporting Online Material

www.sciencemag.org/cgi/content/full/310/5752/1313/DC1
Materials and Methods
Figs. S1 and S2
References

13 September 2005; accepted 1 November 2005
10.1126/science.1120130

Atmospheric Methane and Nitrous Oxide of the Late Pleistocene from Antarctic Ice Cores

Renato Spahni,[1] Jérôme Chappellaz,[2] Thomas F. Stocker,[1]* Laetitia Loulergue,[2] Gregor Hausammann,[1] Kenji Kawamura,[1]† Jacqueline Flückiger,[1]‡ Jakob Schwander,[1] Dominique Raynaud,[2] Valérie Masson-Delmotte,[3] Jean Jouzel[3]

The European Project for Ice Coring in Antarctica Dome C ice core enables us to extend existing records of atmospheric methane (CH_4) and nitrous oxide (N_2O) back to 650,000 years before the present. A combined record of CH_4 measured along the Dome C and the Vostok ice cores demonstrates, within the resolution of our measurements, that preindustrial concentrations over Antarctica have not exceeded 773 ± 15 ppbv (parts per billion by volume) during the past 650,000 years. Before 420,000 years ago, when interglacials were cooler, maximum CH_4 concentrations were only about 600 ppbv, similar to lower Holocene values. In contrast, the N_2O record shows maximum concentrations of 278 ± 7 ppbv, slightly higher than early Holocene values.

Earth's climate during the late Pleistocene was characterized by ice age cycles with relatively short warm periods (interglacials) and longer cold periods (glacials) (*1*). The Vostok ice core provided an archive of climate and atmospheric composition over the past four climatic cycles back to marine isotope stage (MIS) 11, about 420 thousand years before the present (420 kyr B.P.) (*2*). That record demonstrated the high correlation of temperature changes with greenhouse gas concentration changes in the atmosphere in the past. The European Project for Ice Coring in Antarctica (EPICA) Dome Concordia (Dome C) ice core (75°06′S, 123°21′E, 3233 m above sea level) provides an ice core archive much longer, spanning eight climatic cycles over the past 740 thousand years (ky) (*3*). It demonstrates that the oldest four interglacials were cooler but lasted longer than the younger interglacials. Such findings raise the question whether the greenhouse gases CH_4 and N_2O behaved differently before MIS 11. Here, we present CH_4 and N_2O records derived from the EPICA Dome C ice cores reaching back to 650 kyr B.P.

[1]Climate and Environmental Physics, Physics Institute, University of Bern, Sidlerstrasse 5, CH-3012 Bern, Switzerland. [2]Laboratoire de Glaciologie et Géophysique de l'Environnement (LGGE, CNRS-UJF), CNRS, 54 Rue Molières, 38402 St. Martin d'Hères, Grenoble, France. [3]Institut Pierre Simon Laplace/Laboratoire des Sciences du Climat et de l'Environnement, CEA-CNRS 1572, CE Saclay, Orme des Merisiers, 91191 Gif-sur-Yvette, France.

*To whom correspondence should be addressed: stocker@climate.unibe.ch
†Present address: Scripps Institution of Oceanography, University of California, San Diego, 9500 Gilman Drive, La Jolla, CA 92093–0244, USA.
‡Present address: Institute of Arctic and Alpine Research, University of Colorado at Boulder, 450 UCB Boulder, Colorado 80309–0450, USA.

Extracting air from bubbles trapped in polar ice enables us to reconstruct directly the past composition of the atmosphere. The records of CH_4 and N_2O over the past thousand years (*4–6*), the Holocene (*7, 8*), the transition from the last glacial maximum (LGM) to the Holocene (*6, 9*), parts of the last glacial period (*10–14*), and the last four glacial-interglacial cycles (*2, 15–17*) have provided important information about environmental changes in response to regional and global climate variations. Variations in the concentration of globally well-mixed atmospheric CH_4 are attributed to variations in the extent and the productivity of natural wetlands, the main natural sources (*18*). Similarly, variations in the atmospheric N_2O burden are thought to be dominated by variations in the global source strength. About two-thirds of the total preanthropogenic N_2O sources are terrestrial soils, and one-third are nitrification and denitrification processes in the ocean (*13*).

We present high-resolution records of CH_4 and N_2O covering MISs 2 to 7 (Fig. 1), to compare with existing records, and MISs 11 to 16 (Fig. 2), to extend the records back to an age of 650 kyr B.P. Measurements were performed along the EPICA Dome C ice cores (EDC96 and EDC99) at 553 and 476 different depth levels for CH_4 and N_2O, respectively, at the University of Bern and at Laboratoire de Glaciologie et Géophysique de l'Environnement (LGGE) (*19*). The mean CH_4 time resolution is 770 years for MISs 2 to 7 and 840 years for MISs 11 to 16. All ages and their uncertainties are based on the EPICA EDC2 gas and ice age scales (*3*). N_2O analyses were performed only at Bern. Their resolution is similar for MISs 2 to 7 (760 years) but lower for MISs 12 to 16 (1110 years). To be consistent with existing Dome C data, offset corrections for both gases and both laboratories have been applied (*19*).

The Dome C N_2O record is disturbed by artifacts in certain depth intervals as in other ice cores (*6, 13, 17, 20*). High scattering of N_2O values is observed in depth intervals with elevated dust concentrations (*19*) (figs. S1 and S2) during parts of the cold periods MISs 2, 4, 6, 12, 14, and 16 (fig. S3). The EPICA Dome C dust record (*19*) is used to define depth intervals where the dust concentration exceeds 300 ppbw (parts per billion by weight). N_2O measurements in these depths are considered to be disturbed by artifacts and excluded from the record (fig. S3). The good agreement of the remaining record with records measured along other ice cores (Fig. 1) with different characteristics in the concentration of chemical impurities (*6, 13, 14, 17*) supports the assumption that this record shows atmospheric concentrations of the past. Although all samples might be contaminated at some level, no outliers are observed during the

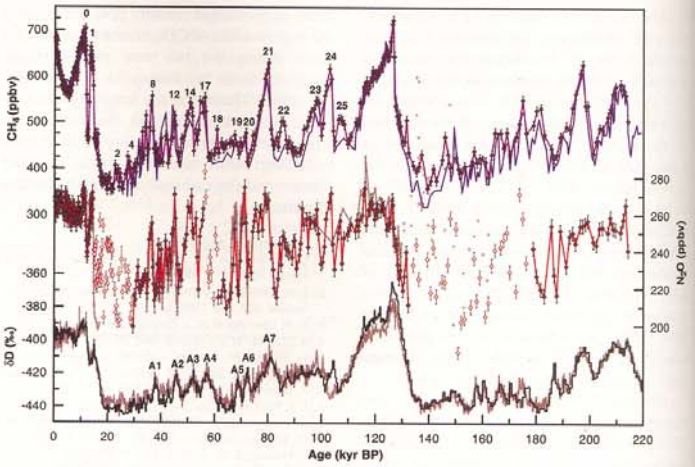

Fig. 1. Dome C CH_4 (purple line), N_2O (red line), and δD (black line) (*3*) records over the past 220 ky. Also shown are Vostok CH_4 data (blue line) (*2, 15*) and δD data (gray line) (*2*). Vostok δD data were increased by 42‰ for better comparison. The Vostok CH_4 and δD records were individually synchronized to Dome C using wiggle matching (*35*). N_2O artifacts (open red diamonds) are separated from the N_2O record (red filled diamonds) with the aid of the dust record (figs. S1 to S3). Additionally, N_2O records published earlier (gray lines and crosses) (*6, 13, 17*), matched by CH_4 to Dome C, are shown for comparison. Error bars represent the 1 SD measurement uncertainty. Dome C CH_4 and N_2O data over the Holocene (*8*), the transition (*9, 36*), and the LGM (*20, 36*) are included in this data set. Dome C measurements covering the time period 0 to 40 kyr B.P. (depth interval 99.5 to 783.8 m) were performed along the EDC96 core, whereas older samples are from the EDC99 core. Numbers 0 to 25 above the CH_4 record denote D/O events (*23*), and A1 to A7 denote Antarctic warming events (*37*). Data are plotted on the EDC2 time scale (*3*).

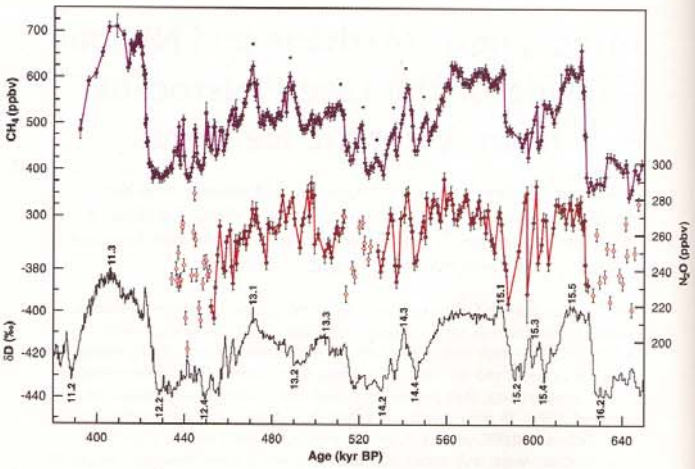

Fig. 2. Dome C CH_4 (purple line) and N_2O (red line) records over the period of MISs 11 to 16, together with high-resolution δD data from Dome C (*24*) (black line). CH_4 measurements performed at Bern are shown as purple diamonds, whereas LGGE measurements are shown as purple circles. N_2O artifacts (red open diamonds) are separated from the N_2O record (red filled diamonds) with the aid of the dust record (figs. S1 to S3). Error bars represent the 1 SD measurement uncertainty. Dome C CH_4 data over termination V (*3*) is included in this data set. Parts of the CH_4 record marked with a star (*) are regular events whose amplitude could be strongly influenced by the precession signal as seen in low-to mid-northern latitude summer insolation. MISs are labeled on the bottom (cold stages) and top (warm stages) of the δD record. Data are shown on the EDC2 time scale (*3*).

highly resolved Holocene. This supports our assumption that other interglacials are also likely free from artifacts.

The Dome C CH_4 data over the last two glacial cycles (Fig. 1) are in good agreement with the Vostok CH_4 record (*15*, *19*), as well as Greenland CH_4 records, when taking into account the interpolar difference (*7*, *21*) and the signal attenuation at low accumulation sites (*22*). The Dome C CH_4 data over the last glacial period confirm the close relation with the 25 Dansgaard/Oeschger (D/O) events as recorded in the North Greenland Ice-Core Project (NGRIP) temperature proxies (*23*). In addition, we find that N_2O also varied during the last glacial period in parallel with the most prominent D/O events (Fig. 1), in agreement with previous results (*6*, *13*, *14*, *16*). N_2O reaches Holocene concentrations of 253 to 272 ppbv (parts per billion by volume) (single values) (*8*) during the maximum of some of these events and during the last interglacial (*14*, *17*). The lowest values found, about 200 ppbv, are similar to those in records published earlier (*13*, *14*). Because the CH_4 and N_2O measurements were performed on the same extracted air samples, a direct comparison without relative time uncertainty is possible between the two gases. The start and end points of single D/O events in CH_4 and N_2O do not necessarily coincide (*13*); e.g., the N_2O concentrations at D/O event 21 start to rise more than 1000 years earlier than CH_4 concentrations. Furthermore, N_2O remains at interglacial values for this specific event, when CH_4 has already dropped to glacial values at the end of the event. The amplitude of some events differs substantially between the two gases as demonstrated by D/O events 19 and 20, also shown in the GRIP record (*13*) (Fig. 1).

The depth interval from 2700 to 3060 m in the EPICA Dome C core permits us to make reconstructions of climate and atmospheric composition for the interval 390 to 650 kyr B.P., most of which precedes the Vostok record (*2*). CH_4 and N_2O measurements performed over this depth interval are shown in Fig. 2, together with high-resolution δD measurements (*24*).

To better characterize warm and cold intervals during the past 650 ky, we refer to "interglacial" as a period during which δD exceeds –403‰ (per mil) (*3*). The use of this definition marks MISs 1, 5.5, 7.3, 7.5, 9.3, and 11.3 as interglacials, which is consistent with the marine records (*1*). In the following, we describe the individual counterparts of the marine stages (*25*) from MISs 16.2 to 11.2.

At 624 kyr B.P., at the end of MIS 16.2, CH_4 falls to a value of 368 ppbv (mean over 7 ky), comparable to the low CH_4 concentration during MIS 6 and MIS 2 in the Dome C record. The increase (termination VII) into MIS 15.5 by about 250 ppbv is smaller than at the younger terminations I, II, IV, and V (*15*). While CH_4 only reaches the mean Holocene (0.3 to 10 kyr B.P.) level of 608 ppbv during MIS 15.1 (600 ppbv, mean over 27 ky) and 15.5 (617 ppbv, mean over 7 ky), the corresponding mean N_2O concentrations of 272 ppbv and 274 ppbv are higher than the Holocene mean (262 ppbv) but similar to early Holocene values. Both records, CH_4 and N_2O, show the distinct separation of MISs 15.1 and 15.5 (Fig. 2) by lower concentrations and three shorter events each during the colder near-glacial periods of MISs 15.2 to 15.4. MIS 15.1 is a surprisingly stable climatic period (1 SD: ± 15 ppbv CH_4, ± 6 ppbv N_2O). Its duration is about 27 ky on the EDC2 age scale. A similar duration is seen in the records of δD (*24*) and CO_2 (*26*); related uncertainties are discussed in (*26*).

In Fig. 3A, δD is plotted together with CO_2 (*26*), CH_4, and N_2O, showing the transition from MISs 14 to 13. During MIS 14, the three gases are closely linked in terms of their timing: Relative maxima (dashed lines) occur at the same time within the data resolution. One of these maxima corresponds to MIS 14.3. CO_2, CH_4, and N_2O seem to lead the δD record and therefore, Antarctic temperature, by about 2000 ± 500 years. However, this could be due to an artifact in the EDC2 time scale, as discussed in Siegenthaler *et al.* (*26*). During MIS 13, the relative CO_2, CH_4, and N_2O maxima are slightly out of phase. In contrast to younger glacial terminations (*2*), the temperatures do not rise directly to a local maximum. Instead, the δD, CO_2, and CH_4 records reveal a transition to the warmest phase (MIS 13.1), which evolves in steps with relapses in between. Nevertheless, sequences of the CO_2 and CH_4 increases to

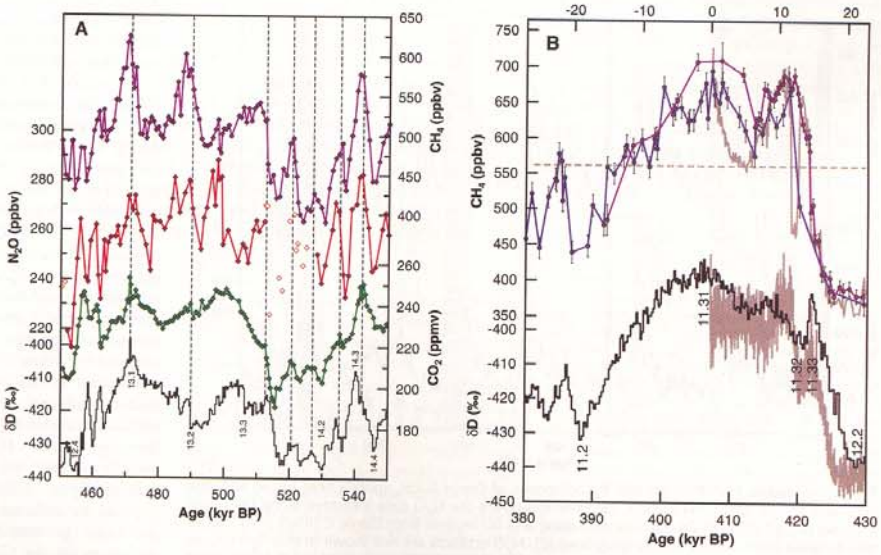

Fig. 3. (A) Dome C CO_2 (*26*) (green line), CH_4 (purple line), and N_2O (red line) records over the period of MISs 13 to 14 as shown in Fig. 2, together with high-resolution δD data from Dome C (*24*) (black line). Vertical dashed lines highlight the coincidence of local CO_2, CH_4, and N_2O maxima. Data are plotted on the EDC2 time scale (*3*). (B) CH_4 records from Dome C (purple line) and Vostok (*15*, *30*) (blue line), together with high-resolution δD data from Dome C (*24*) (black line) covering MIS 11 (labeled at the bottom). The data from MIS 1 are shown as gray lines (time axis on top) for comparison; the curves are aligned by synchronizing the two glacial-interglacial CH_4 increases. Error bars represent the 1 SD measurement uncertainty. Data are plotted on the EDC2 age scale (*3*).

MISs 13.3 and 13.1 look similar to those of the last deglaciation (*9*): CO_2 rises first, CH_4 is delayed, and CO_2 stops rising when CH_4 rises abruptly. In comparison to the last deglaciation, the CH_4 rise at 513 kyr B.P. is rather small. This may be explained by the colder interglacial temperatures that would have favored a relative increase in methanotrophy over methanogenesis, thereby contributing to lowered net CH_4 emissions in the northern extratropics and/or the subtropical and tropical regions. Additionally, the Northern Hemisphere ice sheets may not have retreated as far north during MIS 13. As a consequence, the uncovered areal extent of additional CH_4 source regions was smaller and therefore, the CH_4 overshoot, usually found at terminations, may not have occurred.

At this point, it is difficult to characterize MISs 13 and 15 as interglacials, because the δD values barely exceed –403‰. We therefore refer to these periods as intermediate warm periods (IWP) (*27*). This and their specific evolution of CH_4 suggests that they are similar to MISs 5.1 to 5.3 and MISs 7.1 to 7.3 (*2*) (Fig. 4). In all cases, regular events with CH_4 amplitudes of 50 to 140 ppbv occurred, similar to events marked by stars in Fig. 2. The average return time of the events during MIS 13 is approximately 20 ky, and they last for 5 to 10 ky. The origin of these fluctuations is probably related to the precession cycle (19 to 23 ky) of summer insolation in mid-low to low northern latitudes, as observed for the CH_4 amplitude during the last glacial period (*13*). The N_2O amplitude appears to be modulated by different mechanisms from those responsible for CH_4, as seen in MISs 13 and 15 (e.g., at 498 and 596 kyr B.P.), where N_2O peaks are quite large despite the small CH_4 peaks. Similar discrepancies are in fact found in the last glacial period, e.g., at D/O events 19 and 20 (*13*).

MIS 12 is believed to be a very cold period showing millennial time-scale variations similar to those observed in the last glacial period (*28*). The Dome C record shows CH_4 variations lasting about 1 to 3 ky, with amplitudes of 40 to 120 ppbv (Fig. 2). In addition, Antarctic warming events of 7 to 19‰ are present in the δD record. Their independent evolution on millennial time scales is an indication that the bipolar seesaw may have been operational also during MIS 12 (*29*), but the resolution of our measurements and the uncertainty in their timing prevent us from drawing final conclusions.

Our CH_4 measurements provide an undisturbed record for the entire MIS 11 (Fig. 3B) and support, except for a small offset (*19*), the recently reconstructed MIS 11 record of Vostok (*30*). This is important for two reasons. First, MIS 11 is the longest warm phase of the Antarctic temperature record over the past 740 ky (*24*), with a mean temperature comparable to the Holocene. CH_4 exceeded the minimum Holocene value of 560 ppbv for more than 28 ky. Second, CH_4 increased to 689 ppbv at termination V, followed by an early decrease for about 5000 years, which is very similar to the early Holocene CH_4 record (gray curves in Fig. 3B). It then rose to the high concentration of about 700 ppbv. Ruddiman (*31*) argued that such a behavior of the CH_4 during the early Holocene is due to early anthropogenic interference and that this would be unique. Our data provide a crucial counterexample to this postulated behavior: The early temporary reduction was clearly not an indication of an impending ice age, which started some 20,000 years later in MIS 11, and the increase after this reduction has been established without human influence.

The good agreement between the Dome C and the Vostok (*15*, *30*) record over MISs 1 to 7 and MIS 11 increases our confidence in the fidelity of a composite record of atmospheric CH_4 over the past 650 ky (Fig. 4). The composite record, established by wiggle matching (*32*), demonstrates, within the resolution of our measurements, that preindustrial atmospheric concentrations of CH_4 reconstructed from two Antarctic ice cores have not exceeded 773 ± 15 ppbv (single values at MIS 9.3) during the past 650 ky. The highest mean N_2O values (278 ppbv ± 7 ppbv) over at least a period of 7 ky covered by our records are found during MIS 15.1, slightly higher than early Holocene values. The differing response to climate change of CH_4 and N_2O during MISs 15.1 and 15.5 suggests that the main source regions and/or strengths may strongly differ during interglacials and IWP. High levels are sustained longer for N_2O than for CH_4 during MISs 5.5, 15.1, and 15.3 (Fig. 4), either due to the release of oceanic N_2O or because N_2O soil sources are also productive under semiarid conditions (*13*).

In general, CH_4 is well correlated with δD on glacial-interglacial time scales (>40 ky), including lower CH_4 concentrations during the IWP than during interglacials of the past 420 ky. At terminations, the amplitude of the CH_4 increase is highly correlated with the corresponding Antarctic temperature (r^2 = 0.80). CH_4 has mainly tropical and Northern Hemisphere sources, but only very small austral sources (mainly open-ocean contributions), which suggests that the generally smaller glacial-interglacial temperature change before 440 kyr B.P. revealed by Dome C δD was also of global importance at that time (*33*). The precessional insolation signal in low- to mid-northern latitudes has a strong influence on the amplitude of CH_4 variations for glacial periods and IWP, but the Northern wetlands, episodically covered by boreal ice sheets and exposed to different precipitation patterns, are likely to contribute to this D/O-like variability of the CH_4 concentration (*21*). Furthermore, sink feedbacks, through changes

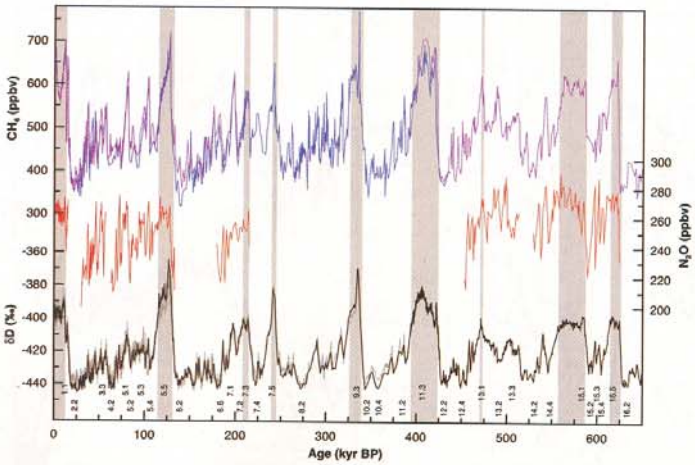

Fig. 4. CH_4 record over the past 650 ky, composed of Dome C CH_4 (purple line) [(*8*, *9*) and new data] and Vostok CH_4 (blue line) (*2*, *15*). Also shown are the N_2O data measured along the Dome C ice cores (red line) [(*8*, *20*, *36*) and new data] and δD records from Dome C (black line) (*24*) as well as those from Vostok +42‰ (gray line) (*2*). N_2O artifacts are not shown in this figure. Gray shaded areas highlight interglacial periods with a δD value >–403‰ as defined in (*3*). Numbers of MISs are given at the bottom of the figure (*25*). Data are shown on the EDC2 time scale (*3*).

of hydrocarbon emissions from the terrestrial biosphere, could have been considerable (*34*).

References and Notes

1. L. E. Lisiecki, M. E. Raymo, *Paleoceanography* **20**, PA1003 (2005).
2. J. R. Petit *et al.*, *Nature* **387**, 359 (1999).
3. EPICA Community Members, *Nature* **431**, 147 (2004).
4. T. Blunier *et al.*, *Geophys. Res. Lett.* **20**, 2219 (1993).
5. D. M. Etheridge, L. P. Steele, R. J. Francey, R. L. Langenfelds, *J. Geophys. Res.* **103**, 15979 (1998).
6. J. Flückiger *et al.*, *Science* **285**, 227 (1999).
7. J. Chappellaz *et al.*, *J. Geophys. Res.* **102**, 15987 (1997).
8. J. Flückiger *et al.*, *Global Biogeochem. Cycles* **16**, 1010 (2002).
9. E. Monnin *et al.*, *Science* **291**, 112 (2001).
10. T. Blunier *et al.*, *Nature* **394**, 739 (1998).
11. E. J. Brook, T. Sowers, J. Orchardo, *Science* **273**, 1087 (1996).
12. J. Chappellaz *et al.*, *Nature* **366**, 443 (1993).
13. J. Flückiger *et al.*, *Global Biogeochem. Cycles* **18**, GB1020 (2004).
14. T. Sowers, R. B. Alley, J. Jubenville, *Science* **301**, 945 (2003).
15. M. Delmotte *et al.*, *J. Geophys. Res.* **109**, D12104 (2004).
16. K. Kawamura, thesis, Tohoku University, Tohoku, Japan (2000).
17. T. Sowers, *J. Geophys. Res.* **106**, 31903 (2001).
18. J. Chappellaz, I. Y. Fung, A. M. Thompson, *Tellus* **45B**, 228 (1993).
19. Materials and methods are available as supporting material on *Science* Online.
20. B. Stauffer, J. Flückiger, E. Monnin, T. Nakazawa, S. Aoki, *Mem. Natl. Inst. Polar Res.* **57**, 139 (2003).
21. A. Dällenbach *et al.*, *Geophys. Res. Lett.* **27**, 1005 (2000).
22. R. Spahni *et al.*, *Geophys. Res. Lett.* **30**, 1571 (2003).
23. NorthGRIP Project Members, *Nature* **431**, 147 (2004).
24. J. Jouzel, in preparation.
25. M. Sarnthein, R. Tiedemann, *Paleoceanography* **5**, 1 (1990).
26. U. Siegenthaler *et al.*, *Science* **310**, 1313 (2005).
27. For MISs 13.1, 13.3, 15.1, and 15.5, δD barely exceeds −403‰, so we use the term intermediate warm period (IWP) for those periods with a lower δD that is still above −425‰ (minimum at MIS 13.2 in Fig. 2). This applies also to MISs 5.1, 5.3, 7.1, and 7.3.
28. D. W. Oppo, J. F. McManus, J. L. Cullen, *Science* **279**, 1335 (1998).
29. T. F. Stocker, S. J. Johnsen, *Paleoceanography* **18**, 1087 (2003).
30. D. Raynaud *et al.*, *Nature* **436**, 39 (2005).
31. W. F. Ruddiman, *Clim. Change* **61**, 261 (2003).
32. The synchronization of the Vostok to the longer Dome C record first has been wiggle matched (*35*) by δD. Then, Vostok gas ages are calculated using Vostok age A55 (*15*), refined by directly matching (*35*) CH_4 from Vostok to Dome C in overlapping periods.
33. V. Masson-Delmotte *et al.*, in preparation.
34. P. J. Valdes, D. J. Beerling, C. E. Johnson, *Geophys. Res. Lett.* **32**, L02704 (2005).
35. J. Schwander *et al.*, *J. Geophys. Res.* **102**, 19483 (1997).
36. B. Stauffer *et al.*, *Ann. Glaciol.* **35**, 202 (2002).
37. T. Blunier, E. J. Brook, *Science* **291**, 109 (2001).

38. We thank U. Siegenthaler, F. Lambert, T. Blunier, and B. Stauffer for discussions and two anonymous reviewers for their comments. This is EPICA publication no. 134. This work is a contribution to the European Project for Ice Coring in Antarctica (EPICA), a joint ESF (European Science Foundation)/European Commission (EC) scientific program, funded by the EC and by national contributions from Belgium, Denmark, France, Germany, Italy, the Netherlands, Norway, Sweden, Switzerland, and the United Kingdom. We acknowledge long-term financial support by the Swiss National Science Foundation and the Swiss Federal Office of Energy for both science and logistic contributions to EPICA and to the University of Bern. Support was also provided by the French program PNEDC (INSU-CNRS), and the EC project EPICA-MIS.

Supporting Online Material

www.sciencemag.org/cgi/content/full/310/5752/1317/DC1

Materials and Methods
Figs. S1 to S3
References

13 September 2005; accepted 2 November 2005
10.1126/science.1120132

Assistance of Microbial Glycolipid Antigen Processing by CD1e

Henri de la Salle,[1*] Sabrina Mariotti,[2*] Catherine Angenieux,[1*] Martine Gilleron,[3*] Luis-Fernando Garcia-Alles,[4] Dag Malm,[5] Thomas Berg,[6] Samantha Paoletti,[2] Blandine Maître,[1] Lionel Mourey,[4] Jean Salamero,[7] Jean Pierre Cazenave,[8] Daniel Hanau,[1] Lucia Mori,[2] Germain Puzo,[3]† Gennaro De Libero[2]†

Complexes between CD1 molecules and self or microbial glycolipids represent important immunogenic ligands for specific subsets of T cells. However, the function of one of the CD1 family members, CD1e, has yet to be determined. Here, we show that the mycobacterial antigens hexamannosylated phosphatidyl-*myo*-inositols (PIM_6) stimulate CD1b-restricted T cells only after partial digestion of the oligomannose moiety by lysosomal α-mannosidase and that soluble CD1e is required for this processing. Furthermore, recombinant CD1e was able to bind glycolipids and assist in the digestion of PIM_6. We propose that, through this form of glycolipid editing, CD1e helps expand the repertoire of glycolipidic T cell antigens to optimize antimicrobial immune responses.

Particular subsets of T cells recognize lipidic and glycolipidic antigens presented by CD1a, b, c, or d proteins, which are antigen-presenting molecules structurally similar to major histocompatibility complex (MHC) class I proteins (*1*). However, unlike classical MHC molecules, CD1 proteins are functionally nonpolymorphic and expressed in a restricted number of cell types, including myeloid dendritic cells (DCs) (*2*). Each CD1 isotype can be characterized by a distinct intracellular trafficking pathway, which allows the capture of lipid antigens either in late or early endosomal compartments (*2*). In particular, CD1b binds glycolipid antigens in MHC class II–enriched lysosomes (*3*) and returns to the plasma membrane to stimulate antigen-specific T cells.

CD1-presented lipid antigens can be of self (*4–7*) or microbial (*8–14*) origin and can include one or more acyl appendages that anchor into the hydrophobic pockets of CD1 protein, as well as a polar moiety directed out toward the T cell receptor (TCR). Exposed amino acids present in α helices of CD1 molecules, together with polar groups of the antigen, directly interact with the TCR and thus constrain the space between CD1 and TCR (*7*, *12*, *15*, *16*). Because such constraint is likely to prevent accommodation and recognition of antigens with large polar heads, it is generally accepted that antigenic glycolipids and lipoglycans with large oligosaccharide moieties are first processed so that T cell recognition can take place.

Relatively little is known about the molecular mechanisms of glycolipid processing. However, previous work has demonstrated that, to be recognized, the oligosaccharide moiety of Gal(α1→2)GalCer must first be cleaved by the lysosomal α-galactosidase (*17*) in the presence of lipid transfer proteins (LTPs) known as saposins, which are involved in the catabolism of endogenous glycolipids (*18*).

Some species express a particular CD1 isoform, CD1e, which has remained the only member of this protein family with undetermined function. CD1e molecules mainly localize within Golgi compartments of

[1]INSERM, U725, Etablissement Francais du Sang-Alsace, F-67065 Strasbourg, France. [2]Experimental Immunology, Department of Research, Basel University Hospital, CH-4031 Basel, Switzerland. [3]CNRS, UMR 5089, Immunochimie et Glycoconjugués Mycobacteriens, and [4]Biophysique Structurale, Département Mécanismes Moléculaires des Infections Mycobactériennes, Institut de Pharmacologie et de Biologie Structurale, F-31077 Toulouse Cedex, France. [5]Department of Medicine and [6]Department of Pathology, University Hospital of Northern Norway, N-9038 Tromsø, Norway. [7]CNRS, UMR 144, Institut Curie, F-75005 Paris, France. [8]INSERM, U311, Etablissement Francais du Sang-Alsace, F-67065 Strasbourg, France.

*These authors contributed equally to this work.
†To whom correspondence should be addressed. E-mail: gennaro.delibero@unibas.ch (G.D.L); germain.puzo@ipbs.fr (G.P.)